Supplementary Material

Experimental Details

1. Synthesis of g-C_3N_4

For a typical run, 5 g melamine was transferred into a quartz boat and kept in air tube furnace at 550 ℃ for 4 h at a heating rate of 6 ℃·min [1].

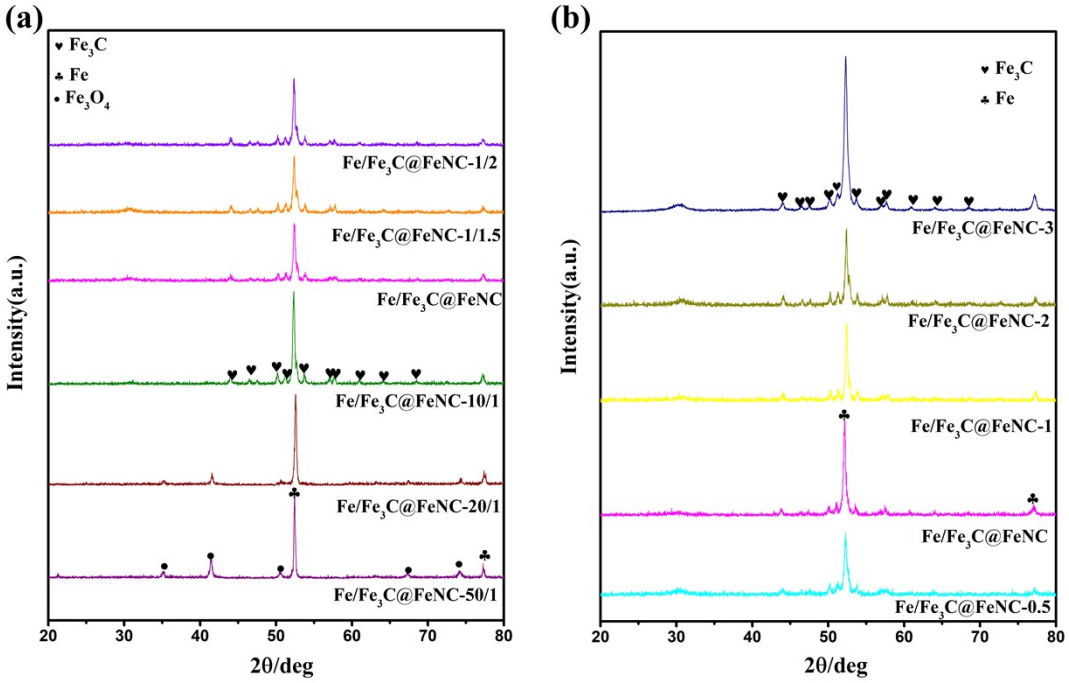

Fig. S1. (a) XRD patterns of the Fe-N-C samples prepared by different mass ratios of Fe_2O_3@PDA and g-C_3N_4 from 50/1 to 1/2, (b) XRD patterns of Fe/Fe_3C@FeNC obtained by different pyrolysis durations from 0.5 h to 3 h.

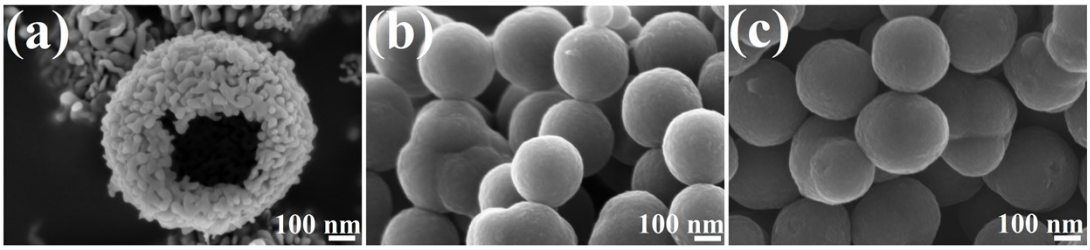

Fig. S2. SEM images of (a) Fe_2O_3, (b) NC-P, (c) NC

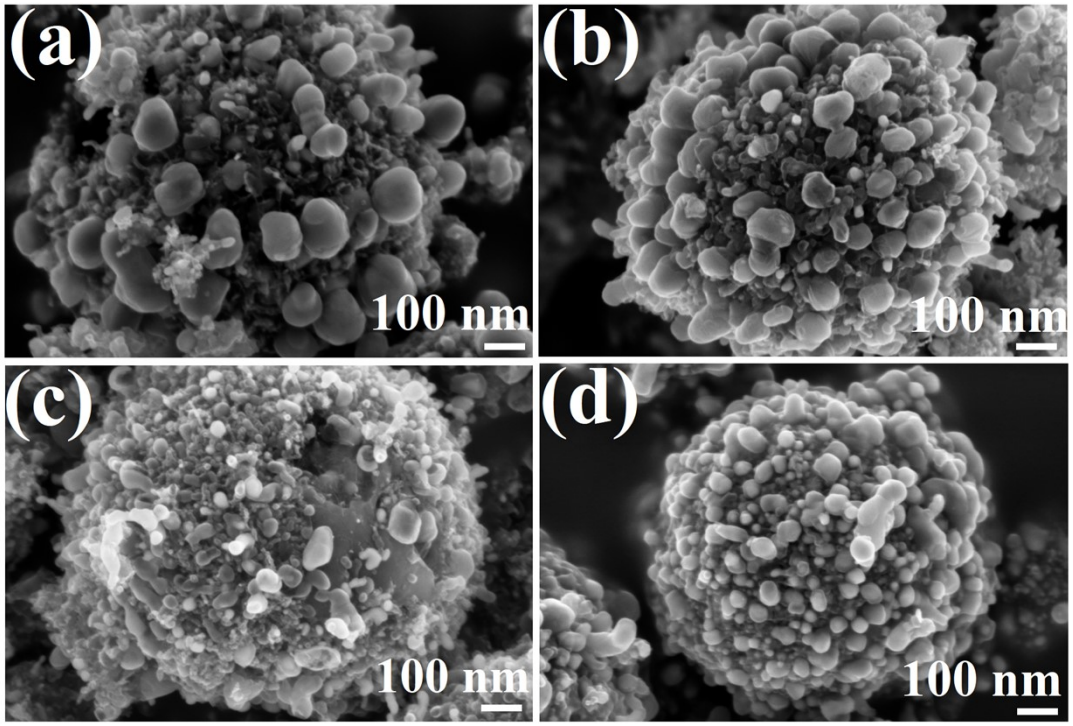

Fig. S3. SEM images of (a) Fe/Fe_3C@FeNC-0.5, (b) Fe/Fe_3C@FeNC-1, (c) Fe/Fe_3C@FeNC-2, (d) Fe/Fe_3C@FeNC-3.

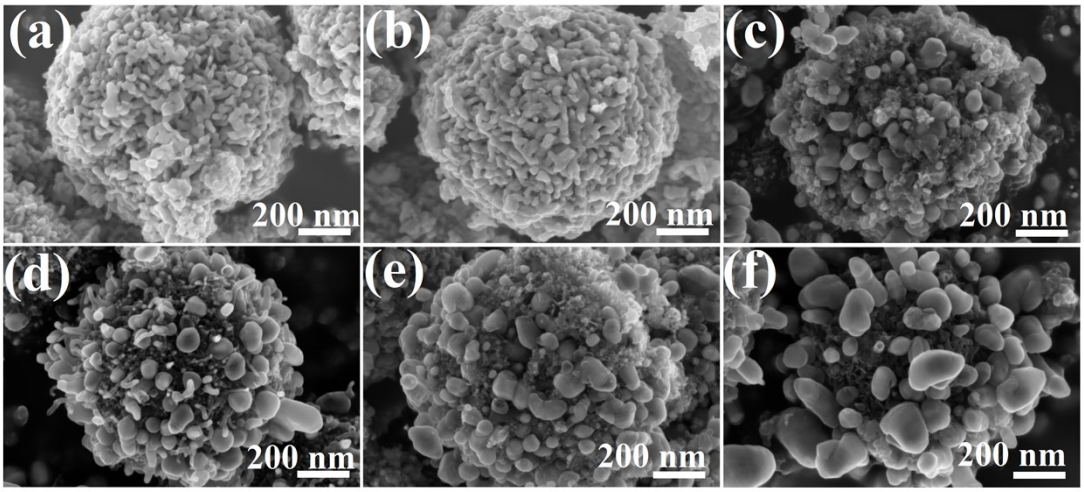

Fig. S4. SEM images of (a) Fe/Fe_3C@FeNC-50/1, (b) Fe/Fe_3C@FeNC-20/1, (c) Fe/Fe_3C@FeNC-10/1, (d) Fe/Fe_3C@FeNC, (e) Fe/Fe_3C@FeNC-1/1.5, (f) Fe/Fe_3C@FeNC-1/2.

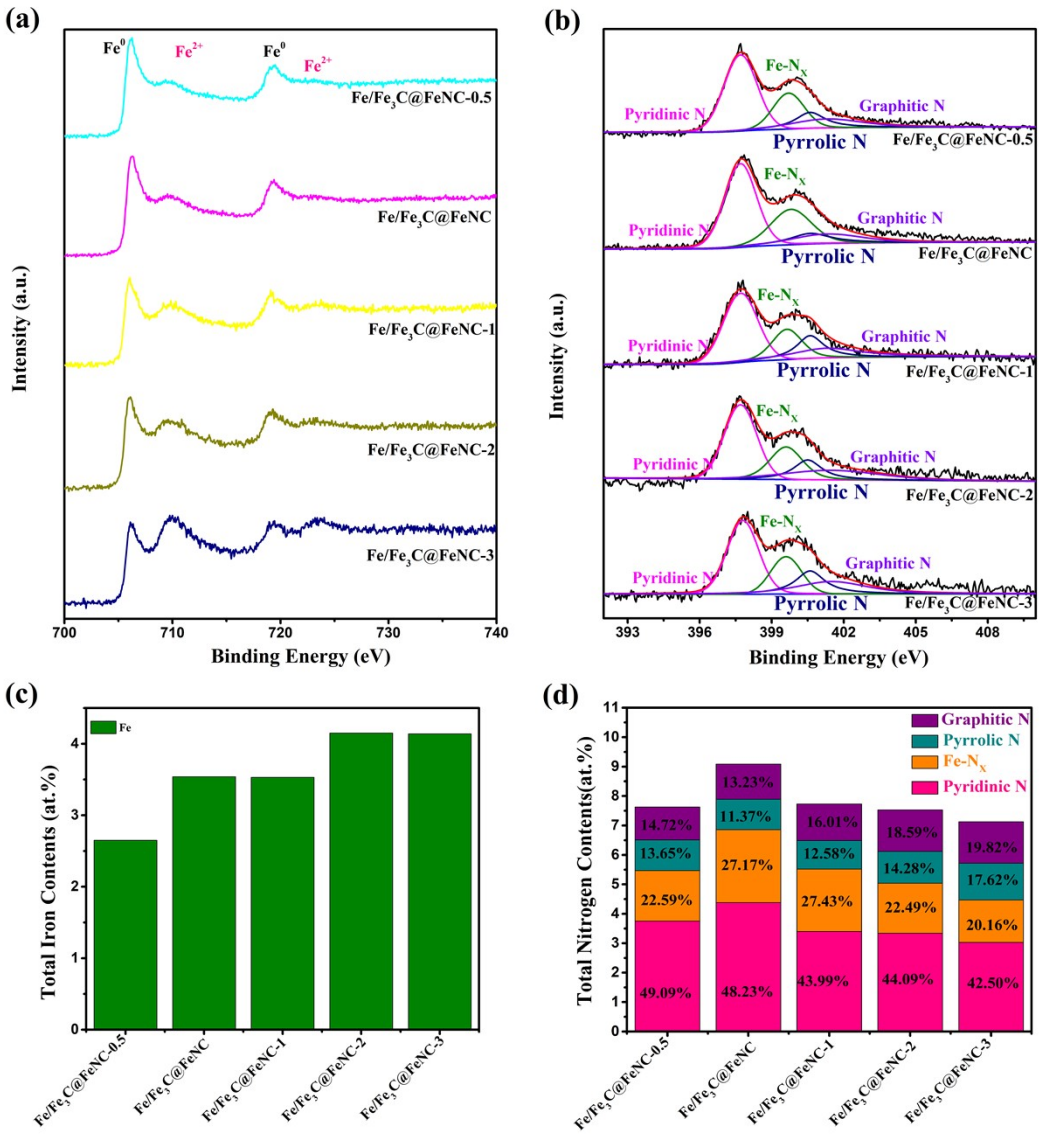

Fig. S5. (a) High-resolution Fe 2p spectrum and (b) high-resolution N 1s spectrum for different pyrolysis durations from 0.5 h to 3 h, (c) The contents of Fe and (d) the contents of total and function N for different pyrolysis durations from 0.5 h to 3 h according to XPS.

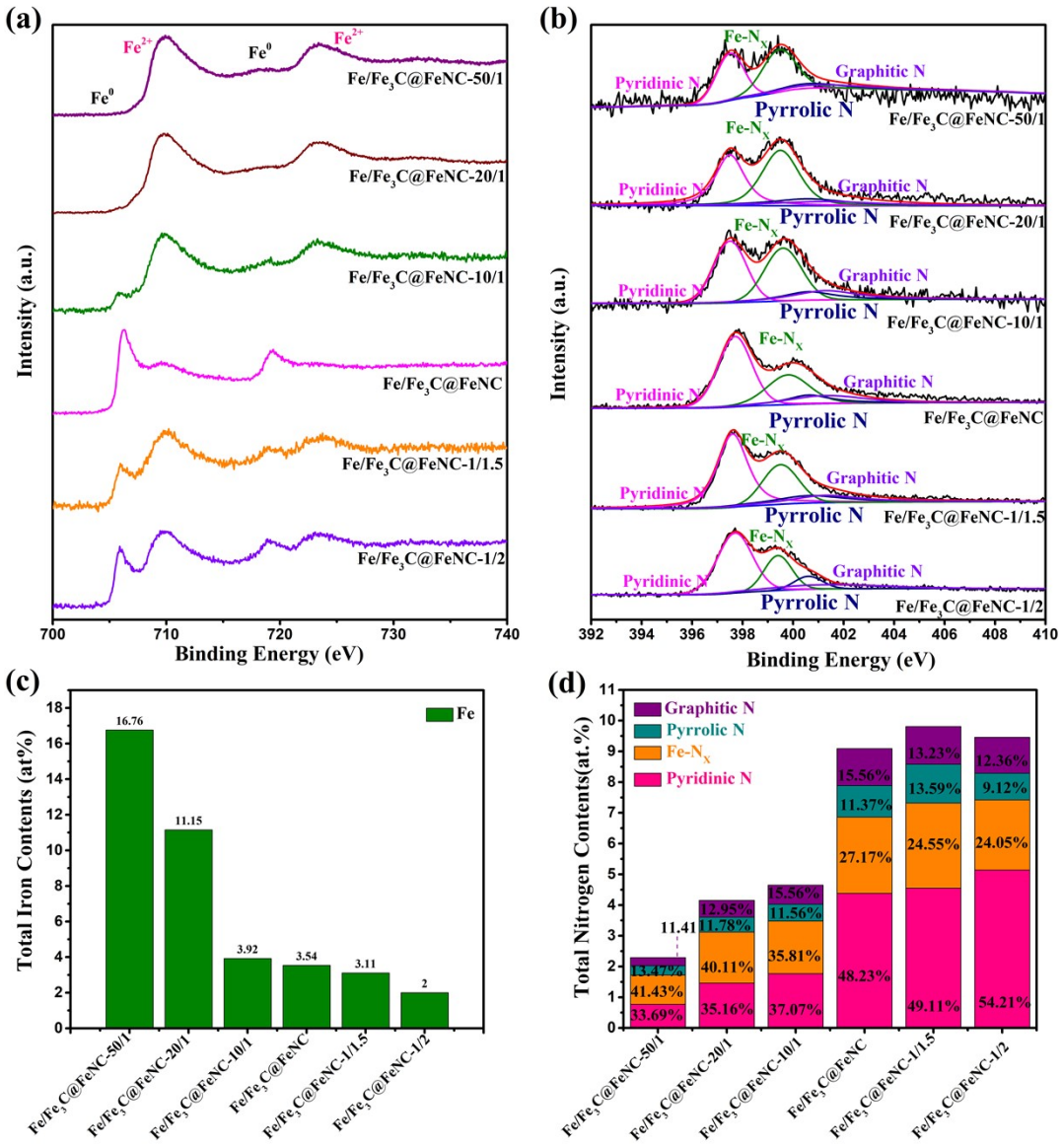

Fig. S6. (a) High-resolution Fe 2p spectrum and (b) high-resolution N 1s spectrum different mass ratios of Fe_2O_3@PDA and g-C_3N_4 from 50/1 to 1/2, (c) The contents of Fe (d) the contents of total and function N for different mass ratios of Fe_2O_3@PDA and g-C_3N_4 from 50/1 to 1/2 according to XPS.

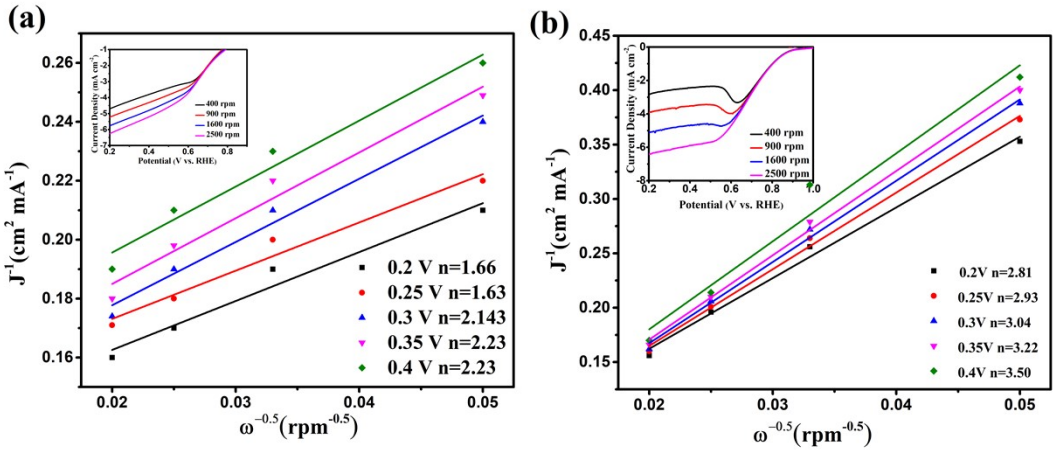

Fig. S7. K-L plots and electron transfer number at various potential of (a) NC, (b) Fe/Fe_3C@FeNC-nP-1/1.

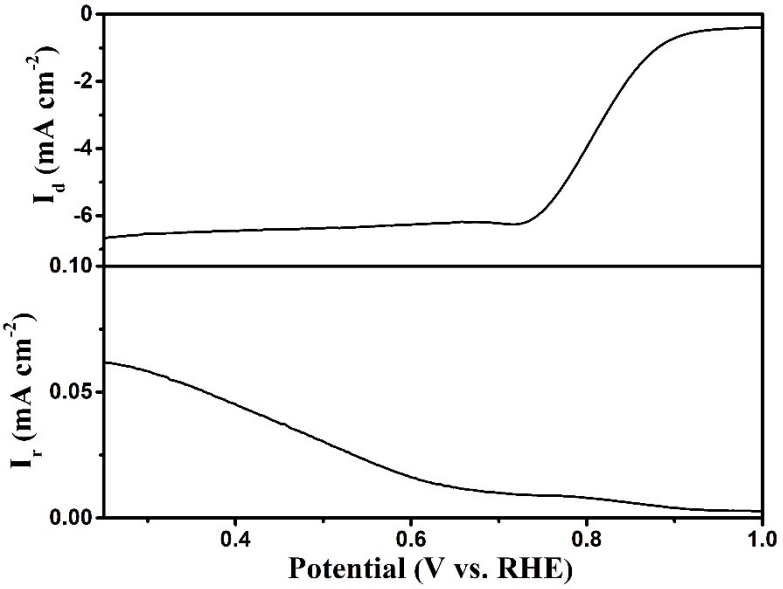

Fig. S8. RRDE voltammograms recorded with Fe/Fe_3C@FeNC in O_2-saturated 0.1 M KOH solution. Scan rate: 10 mV s^{-1} rotation rate 1600 rpm.

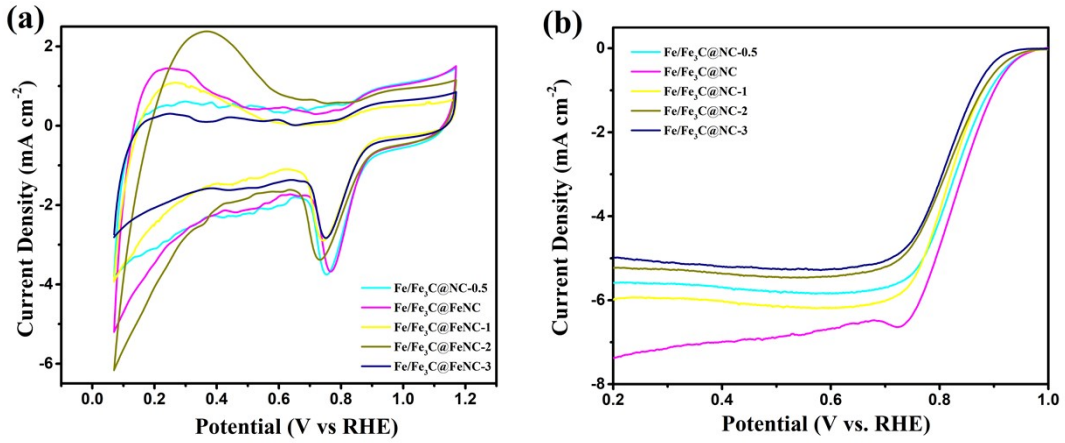

Fig. S9. (a) The CV curves, (b) LSV curves of different pyrolysis durations from 0.5 h to 3 h.

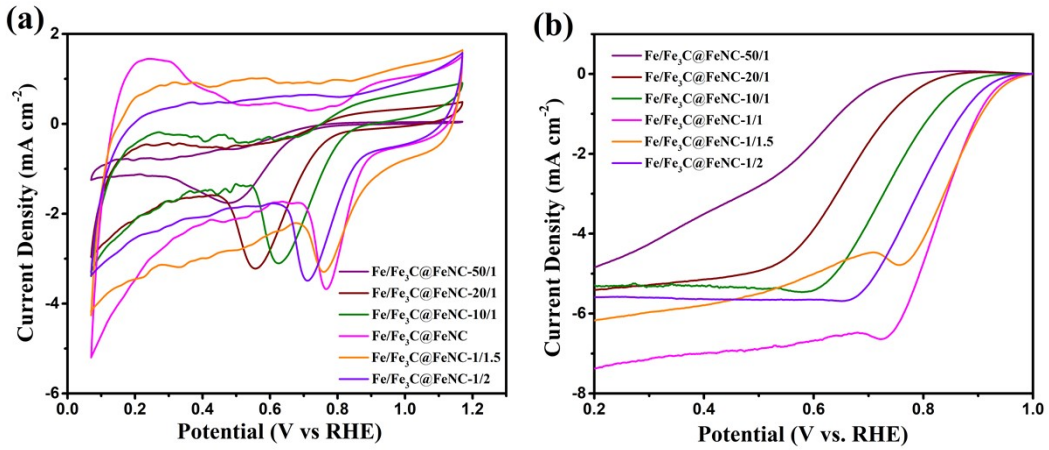

Fig. S10. (a) The CV curves, (b) LSV curves of different mass ratios of Fe_2O_3@PDA and g-C_3N_4 from 50/1 to 1/2.

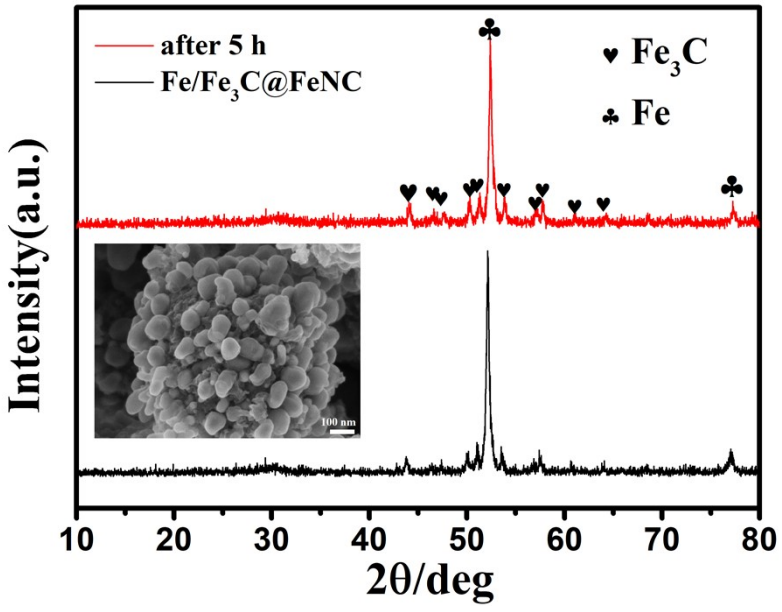

Fig. S11. XRD patterns of different $FeFe_3C$@FeNC and after 5 h cycle, and SEM image of after 5 h cycle

(inset).

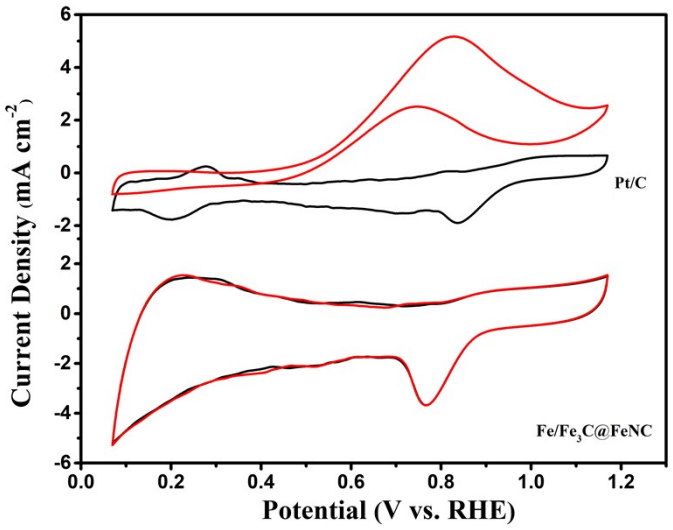

Fig. S12. Methanol tolerance tests of Fe/Fe_3C@FeNC and commercial Pt/C.

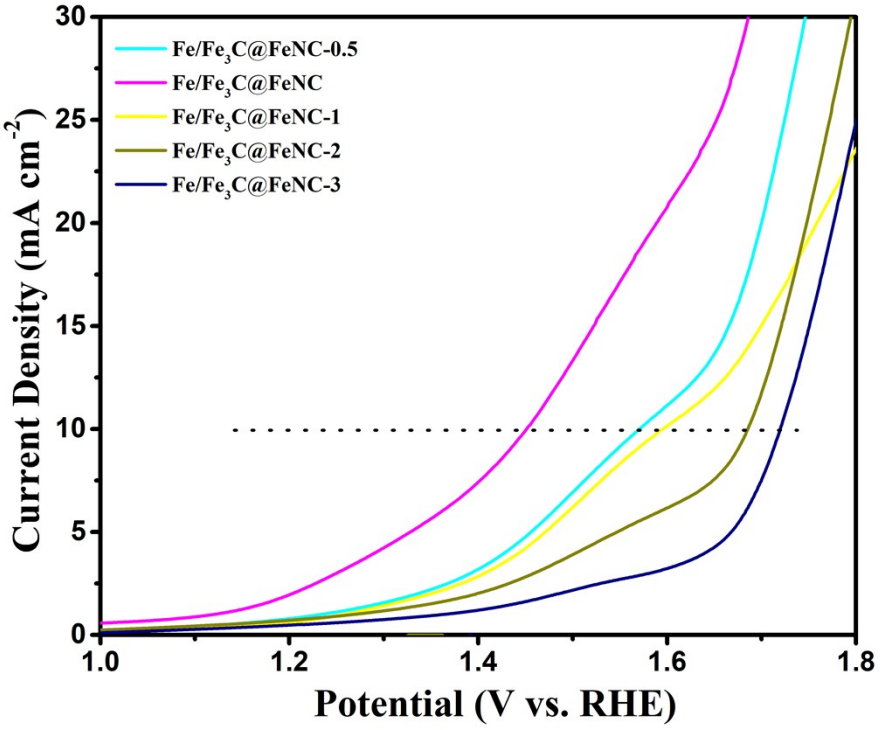

Fig. S13. LSV curves of different pyrolysis durations from 0.5 h to 3 h.

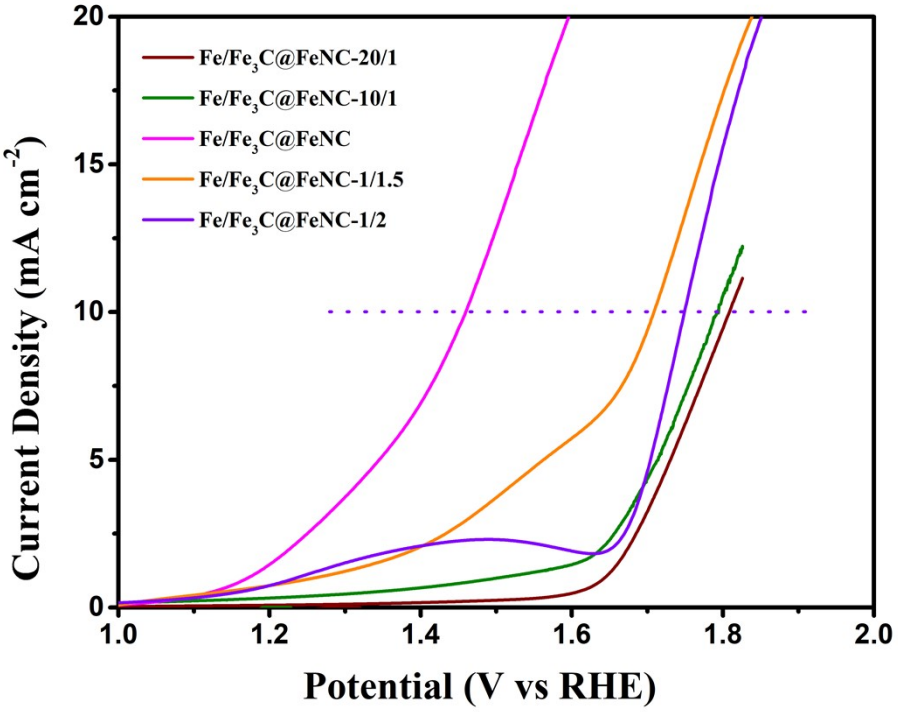

Fig. S14. LSV curves of different mass ratios of Fe_2O_3@PDA and g-C_3N_4 from 20/1 to 1/2.

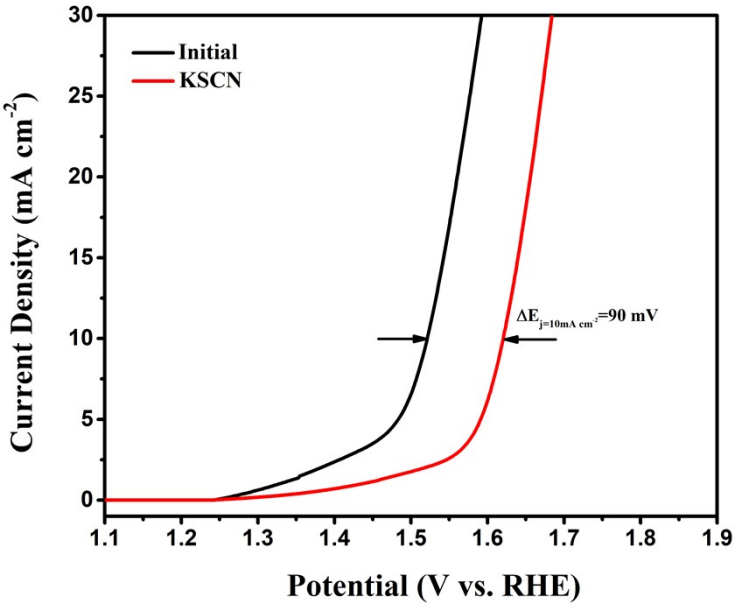

Fig. S15. LSV curves of SCN^{-1} poisoned and initial Fe/Fe_3C@FeNC.

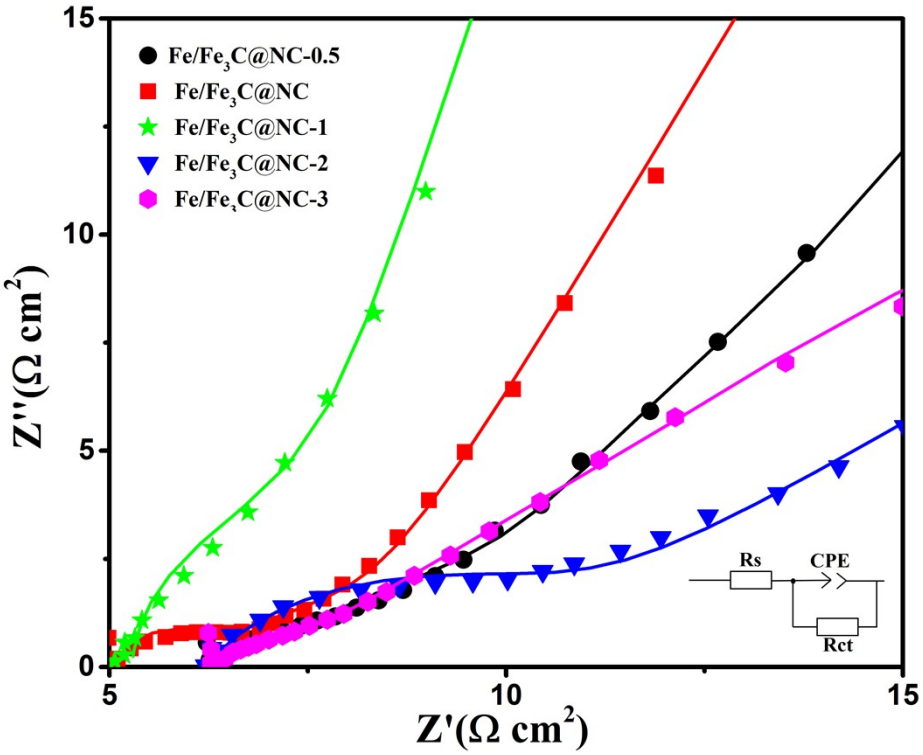

Fig. S16. Nyquist plots of the different pyrolysis durations from 0.5 h to 3 h.

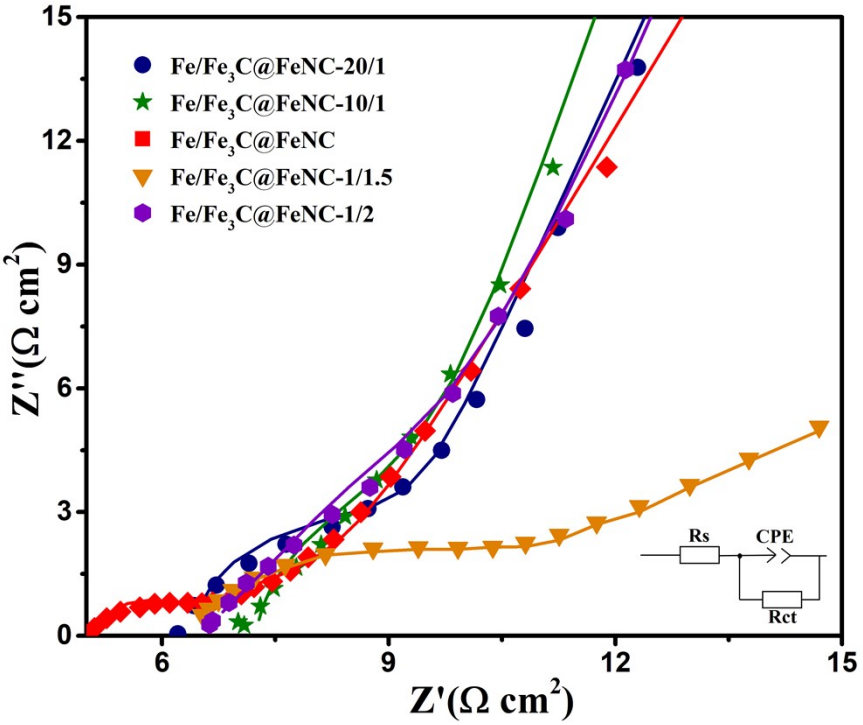

Fig. S17. Nyquist plots of the different mass ratios of Fe_2O_3@PDA and g-C_3N_4 from 20/1 to 1/2.

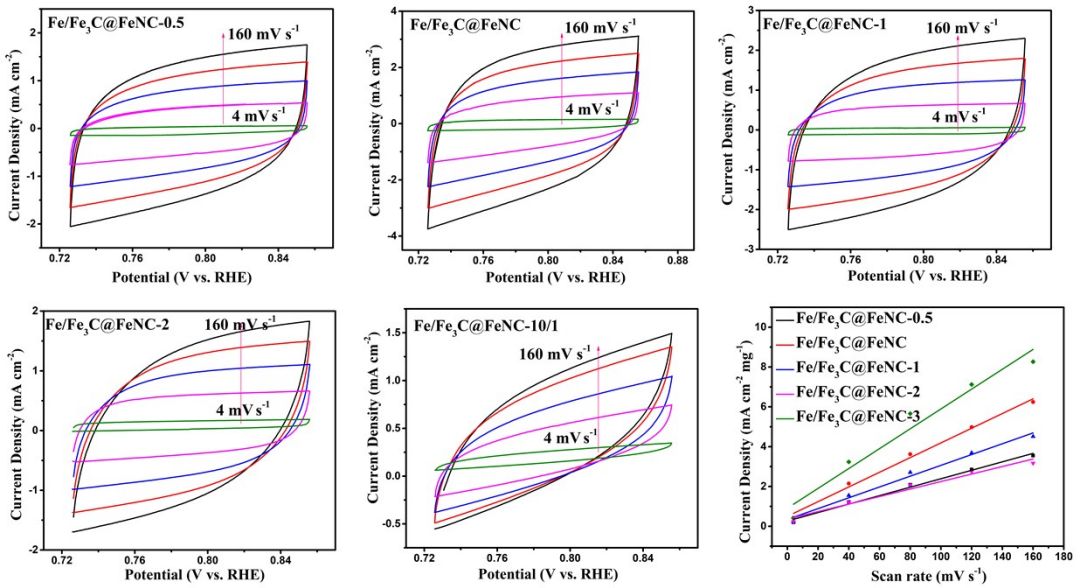

Fig. S18. (a-e) CV curves at different scan rates for different pyrolysis durations from 0.5 h to 3 h. (f) Dependence of current density on scan rate.

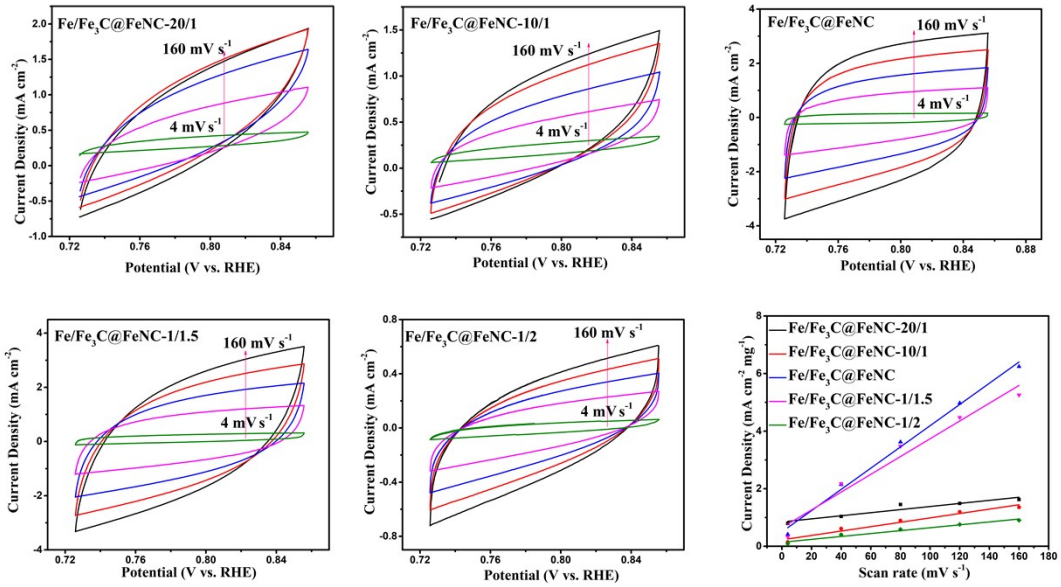

Fig. S19. (a-e) CV curves at different scan rates for different mass ratios of Fe_2O_3@PDA and g-C_3N_4 from 20/1 to 1/2. (f) Dependence of current density on scan rate.

Table S1. ORR and OER performance of Fe/Fe_3C@FeNC in this work and some other Fe-N-C electrocatalysts.

Electrocatalyst	ORR			OER	ΔE (mV)	Reference
	$E_{1/2}$(V)	j_L (mA cm^{-2})	Stability retention rate (%)/Time	η(mV) at j=10 mA cm^{-2}		
Fe/Fe_3C@FeNC	0.832	7.7	94/18000	220	610	This work
Co–Fe–P–Se/NC	0.76	-	60.4/7200	270	740	[2]
FePPc@CB	0.908	7.44	73/40000	388	680	[3]
Fe_3O_4@FeNC	0.890	6.9	90/40000	-	-	[4]
Fe@C-NG/NCNTs	0.840	-	78.4/40000	450	840	[5]
N-Co_3O_4@NC-2	0.77	5.87	97.6/15000	320	780	[6]
Fe_3O_4/N-MCS-2	0.702	5.16	91.6/80000	-	-	[7]
Fe_3C/Fe_2O_3@NGNs	0.82	5.64	99.17/15000	460	868	[8]
FeS/Fe_3C@NS-C-900	0.78	6.83	90/20000	270	720	[9]
Fe–N-DSC	0.739	-	95.9/30000	-	-	[10]
Co_2P@NPC-1	0.828	5.117	88/20000	327	729	[11]

Table S2. Elemental values of fitted equivalent circuit based on EIS spectra for OER.

Catalyst	Rct (Ω·cm^2)	Rs (Ω·cm^2)	CPE-T ($Ω^{-1}$ ·cm^{-2} ·s^{-n})	CPE-P
Fe/Fe_3C@FeNC-0.5	1.18	6.01	0.00015	0.88
Fe/Fe_3C@FeNC	0.61	5.23	1.84E-6	0.87
Fe/Fe_3C@FeNC-1	1.67	5.45	6.74E-6	0.88
Fe/Fe_3C@FeNC-2	3.79	6.20	6.24E-5	0.86
Fe/Fe_3C@FeNC-3	0.56	6.32	5.04E-6	0.87
Fe/Fe_3C@FeNC-20/1	2.22	6.18	1.02E-6	0.88
Fe/Fe_3C@FeNC-10/1	1.52	6.21	8.66E-6	0.89
Fe/Fe_3C@FeNC-1.5/1	9.67	6.25	0.00040	0.86
Fe/Fe_3C@FeNC-1/2	87.27	6.47	0.00014	0.88

Table S3. The performance of ZABs by recently reported bifunctional electrocatalysts and Fe/Fe_3C@FeNC in this work.

Electrocatalyst	Open-circuit voltage (V)	Maximum power density (mW cm^{-2})	Specific capacity (mAh g^{-1})	Energy density (Wh kg^{-1})	Reference
Fe/Fe_3C@FeNC	**1.414**	**134.6**	**856.2**	**1094**	This work
FeNi-N-C/N- CNT	1.46	273	755	924	[12]
Fe_3O_4@NHCS-2	1.42	133	701	-	[13]
Fe_2O_3@NC-450	1.267	156.6	-	-	[14]
Fe_3C/Fe_2O_3@NGNs	1.46	139.8	722	805	[8]
Co–Fe–P–Se/NC	1.3	104	708	805	[2]
FePPc@CB	1.367	90	1391	1317	[3]
FeS/Fe_3C@NS-C-900	1.455	192.2	750	-	[9]
$FeNi_3$@NC	1.14	139	756	915	[15]
nNiFe LDH/3D MPC	1.51	97	573	-	[16]
Co/Co–N–C	1.434	122.5	700.6	897.1	[17]

References

[1] Y.J. Deng, B. Chi, X.L. Tian, Z.M. Cui, E.S. Liu, Q.Y. Jia, et al. g-C3N4 promoted MOF derived hollow carbon nanopolyhedra doped with high density/fraction of single Fe atoms as an ultra-high performance non-precious catalyst towards acidic ORR and PEM fuel cells. J Mater Chem A. 7 (2019) 5020-30.

[2] H.B. Wu, J. Wang, J. Yan, Z.X. Wu, W. Jin. MOF-derived two-dimensional N-doped carbon nanosheets coupled with Co-Fe-P-Se as efficient bifunctional OER/ORR catalysts. Nanoscale. 11 (2019) 20144-50.

[3] W.Z. Cheng, J.L. Liang, H.B. Yin, Y.J. Wang, W.F. Yan, J.N. Zhang. Bifunctional iron-phtalocyanine metal-organic framework catalyst for ORR, OER and rechargeable zinc-air battery. Rare Metals. 39 (2020) 815-23.

[4] S.Q. Hu, W.P. Ni, D.H. Yang, C. Ma, J.H. Zhang, J.F. Duan, et al. Fe3O4 nanoparticles encapsulated in single-atom Fe-N-C towards efficient oxygen reduction reaction: Effect of the micro and macro pores. Carbon. 162 (2020) 245-55.

[5] Q.C. Wang, Y.P. Lei, Z.Y. Chen, N. Wu, Y.B. Wang, B. Wang, et al. Fe/Fe3C@C nanoparticles

encapsulated in N-doped graphene-CNTs framework as an efficient bifunctional oxygen electrocatalyst for robust rechargeable Zn-air batteries. J Mater Chem A. 6 (2018) 516-26.

[6] Z.C. Wang, W.J. Xu, X.K. Chen, Y.H. Peng, Y.Y. Song, C.X. Lv, et al. Defect-Rich Nitrogen Doped Co3O4/C Porous Nanocubes Enable High-Efficiency Bifunctional Oxygen Electrocatalysis. Adv Funct Mater. 29 (2019) 11.

[7] H.T. Wang, W. Wang, M.X. Gui, M. Asif, Z.Y. Wang, Y. Yu, et al. Uniform Fe3O4/Nitrogen-Doped Mesoporous Carbon Spheres Derived from Ferric Citrate-Bonded Melamine Resin as an Efficient Synergistic Catalyst for Oxygen Reduction. ACS Appl Mater Interfaces. 9 (2017) 335-44.

[8] Y.H. Tian, L. Xu, J.C. Qian, J. Bao, C. Yan, H.N. Li, et al. Fe3C/Fe2O3 heterostructure embedded in N-doped graphene as a bifunctional catalyst for quasi-solid-state zinc-air batteries. Carbon. 146 (2019) 763-71.

[9] Y.W. Li, W.J. Zhang, J. Li, H.Y. Ma, H.M. Du, D.C. Li, et al. Fe-MOF-Derived Efficient ORR/OER Bifunctional Electrocatalyst for Rechargeable Zinc-Air Batteries. ACS Appl Mater Interfaces. 12 (2020) 44710-9.

[10] Z. Huang, H.Y. Pan, W.J. Yang, H.H. Zhou, N. Gao, C.P. Fu, et al. In Situ Self-Template Synthesis of Fe-N-Doped Double-Shelled Hollow Carbon Microspheres for Oxygen Reduction Reaction. ACS Nano. 12 (2018) 208-16.

[11] J. Li, G.Y. Liu, B.B. Liu, Z.Y. Min, D. Qian, J.B. Jiang, et al. An extremely facile route to Co2P encased in N,P-codoped carbon layers: Highly efficient bifunctional electrocatalysts for ORR and OER. Int J Hydrog Energy. 43 (2018) 1365-74.

[12] J.J. Fang, X.J. Zhang, X.D. Wang, D. Liu, Y.R. Xue, Z.Y. Xu, et al. A metal and nitrogen doped carbon composite with both oxygen reduction and evolution active sites for rechargeable zinc-air batteries. J Mater Chem A. 8 (2020) 15752-9.

[13] Y.Q. Li, H.Y. Huang, S.R. Chen, X. Yu, C. Wang, T.L. Ma. 2D nanoplate assembled nitrogen doped hollow carbon sphere decorated with Fe3O4 as an efficient electrocatalyst for oxygen reduction reaction and Zn-air batteries. Nano Res. 12 (2019) 2774-80.

[14] Z.R. Xiao, C. Wu, W. Wang, L. Pan, J.J. Zou, L. Wang, et al. Tailoring the hetero-structure of iron oxides in the framework of nitrogen doped carbon for the oxygen reduction reaction and zinc-air batteries. J Mater Chem A. 8 (2020) 25791-804.

[15] D. Chen, J.W. Zhu, X.Q. Mu, R.L. Cheng, W.Q. Li, S.L. Liu, et al. Nitrogen-Doped carbon coupled

FeNi3 intermetallic compound as advanced bifunctional electrocatalyst for OER, ORR and zn-air batteries. Appl Catal B-Environ. 268 (2020) 9.

[16] W. Wang, Y.C. Liu, J. Li, J. Luo, L. Fu, S.L. Chen. NiFe LDH nanodots anchored on 3D macro/mesoporous carbon as a high-performance ORR/OER bifunctional electrocatalyst. J Mater Chem A. 6 (2018) 14299-306.

[17] D. Wang, P.X. Yang, H. Xu, J.Y. Ma, L. Du, G.X. Zhang, et al. The dual-nitrogen-source strategy to modulate a bifunctional hybrid Co/Co-N-C catalyst in the reversible air cathode for Zn-air batteries. J Power Sources. 485 (2021) 10.